Alkoxy Chain Number Effect on Self-Assembly of a Trigonal Molecule at the Liquid/Solid Interface

Kazukuni Tahara,[*,†] *Ruri Nakayama,*[†] *Matsuhiro Maeda,*[†] *Steven De Feyter,*[*,‡] *Yoshito Tobe**[*,¶,#]

[†]Department of Applied Chemistry, School of Science and Technology, Meiji University, 1-1-1 Higashimita, Tama-ku, Kawasaki, Kanagawa, 214-8571, Japan.

[‡]Division of Molecular Imaging and Photonics, Department of Chemistry, KU Leuven, Celestijnenlaan 200 F, 3001 Leuven, Belgium.

[¶]The Institute of Scientific and Industrial Research, Osaka University, Ibaraki, Osaka 567-0047, Japan.

[#]Department of Applied Chemistry, National Chiao Tung University, 1001 Ta Hsueh Road, Hsinchu 30030, Taiwan.

ABSTRACT

We herein investigated the effect of the number of alkoxy chains on the two-dimensional self-assembly of a trigonal molecular building block. To this end, a dehydrobenzo[12]annulene (DBA) derivative, **DBA-OC14-OC1** having three tetradecyloxy chains and three methoxy groups in an alternating manner, was synthesized. Scanning tunneling microscopy (STM) observations at the 1,2,4-trichlorobenzene (TCB)/graphite interface revealed that **DBA-OC14-OC1** forms three monolayer structures, porous honeycomb, parallelogram, and hexagonal A structures. At the 1-phenyloctane (PO)/graphite interface, **DBA-OC14-OC1** also forms three structures: parallelogram, hexagonal B and dense-linear structures. In contrast to the previously reported DBA derivative **DBA-OC14** having six tetradecyloxy chains, **DBA-OC14-OC1** shows structural polymorphism with a variety of alkyl chain interaction modes. Since in the observed patterns **DBA-OC14-OC1** adopts a low symmetric C_s or C_1 geometry, the variation of the interaction modes and the resulting network patterns likely originate from the conformational flexibility on surface of this DBA by decreasing number of alkyl chains. Molecular mechanics simulations gave insight in the structural and energy aspects of this pattern formation. We also discussed the role of solvents, TCB and PO, on the polymorph formation.

INTRODUCTION

Structural control of surface-confined supramolecular self-assembled molecular networks (SAMNs)[1] generates a lot of interest in connection with potential applications such as molecular-scale electronics, sensing, and catalysis.[2–4] Toward a sophisticated control of those structures and functionalities, various molecular building blocks that produce self-assembled networks with different topologies have been investigated. Two typical environments, ultrahigh vacuum (UHV) and liquid/solid interface are often employed to study surface-confined molecular self-assembly.[5,6] In the former environment, molecule-substrate and intermolecular interactions play significant roles for the network formation.[5,7] Molecular dose and substrate temperature influence the resulting self-assembling structures too. At the liquid/solid interface, also solvent-molecule and solvent-substrate interactions are crucial for the structural control.[8–12] Moreover, other factors as well as external stimuli such as solute concentration,[13–16] temperature[17,18] and electric field[19,20] are known to have a strong impact on the resulting self-assembling structures. Scanning tunneling microscopy (STM) techniques offer visualization of these structures at the nanoscale with submolecular resolution in both environments.

Over the past decade, we studied the self-assembly of a family of trigonal molecular building blocks, dehydrobenzo[12]annulene (DBA) derivatives **DBA-OCn**s having six long alkoxy chains, at the liquid/solid interface (Figure 1a).[21,22] For instance, **DBA-OCn**s formed honeycomb type porous and linear type non-porous structures at the 1,2,4-trichlorobenzene (TCB)/graphite interface (Figure

1b).[23] Alkoxy chain length influences the relative stability of these two structures. Moreover, we also reported that these structures can be converted into each other by the modulation of solute concentration and temperature.[13,17] The monolayer structures and their relative stabilities vary depending on the solvent employed.[23,24] While TCB favors the formation of the honeycomb structures most likely due to stabilization by solvent co-adsorption, dense packings are favored in other solvents. The key intermolecular interaction for the monolayer formation of this type of compounds is van der Waals interactions between the interdigitated four alkyl chains, of which each two per molecule participate in the intermolecular connections ([2+2] mode). The optimal interchain distance at the triangular core side is essential for the [2+2] interaction mode.[25]

Here we investigate the effect of the number of alkyl chains on the self-assembly of a trigonal molecule using DBA derivative because of its synthetic versatility in the selection of alkyl chain numbers.[22,26] Such molecular structural changes might lead to drastic changes in the on-surface molecular conformation and the intermolecular as well as molecule-substrate interactions, resulting in a strong impact on the formation of self-assembled structures. In this context, we designed and synthesized **DBA-OC14-OC1** with alternating three tetradecyloxy (OC14) chains and methoxy (OC1) groups, respectively (Figures 1a,c). The long OC14 chain is chosen to ensure appropriate intermolecular and molecule-substrate interactions for the network formation. Moreover, the self-assembly of the reference compound with six OC14 chains, **DBA-OC14** is well studied.[13,23] The six alkyl chains of **DBA-OCn** and its homologues form [2+2], [2+1] and [1+1] interaction modes.[23,27]

Upon reducing the alkyl chain number, additional interaction modes are expected, as the chains gain enhanced conformational freedom due to the increased free space around the trigonal core. This free space could potentially be occupied by solvent molecules too and thus the choice of the solvent is expected to have an impact on the self-assembled structures.[28] While the self-assembly of molecules with a hexagonal or trigonal core substituted with three long alkyl chains was reported,[29–31] this study highlights the effect of the number of alkyl chains on the self-assembly.

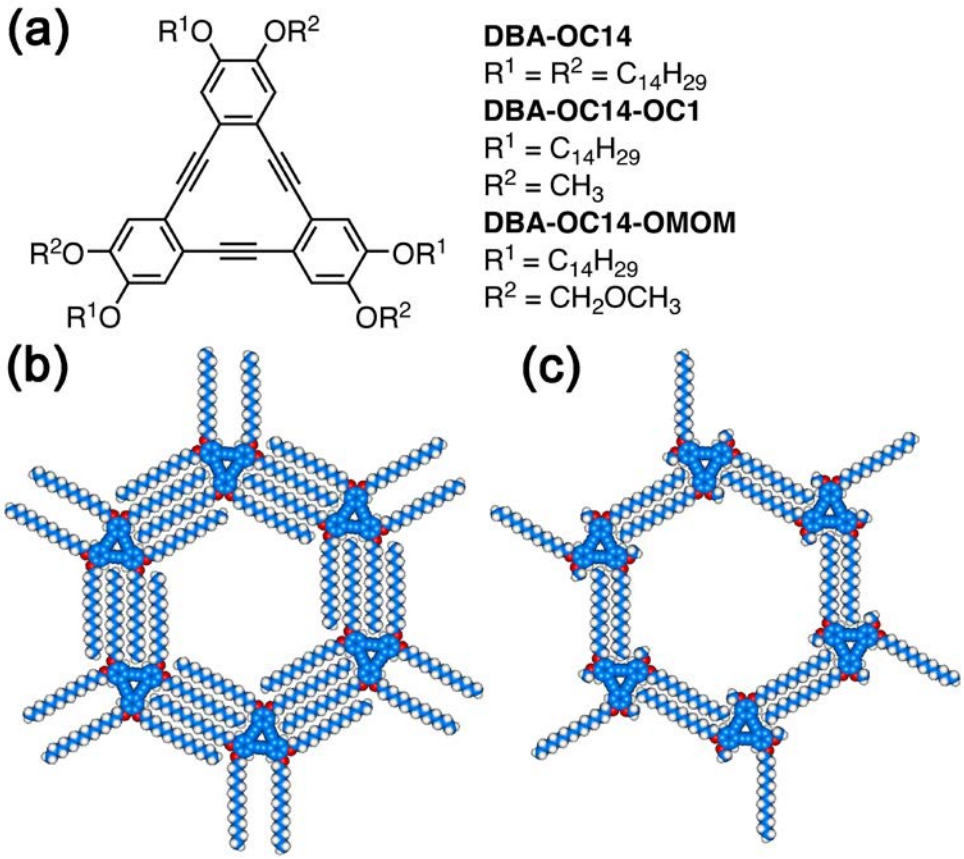

Figure 1. (a) Chemical structures of **DBA-OC14**, **DBA-OC14-OC1** and **DBA-OC14-OMOM**. (b, c) Molecular models of honeycomb structures formed by **DBA-OC14** (b) and **DBA-OC14-OC1** (c), respectively.

METHODS

Synthesis of DBA-OC14-OC1. The synthesis of **DBA-OC14-OC1** was conducted according to a previously reported method (Scheme S1).[32] Details are described in Supporting Information.

STM Observation. All experiments were performed at 20–26 °C using a Nanoscope IIID or V (Bruker AXS) with an external pulse/function generator (Agilent 33220A) with negative sample bias. STM tips were mechanically cut from Pt/Ir wire (80%/20%, diameter 0.25 mm).

Prior to imaging, a compound under investigation was dissolved in distilled commercially available 1,2,4-trichlorobenzene (Nacalai Tesque) or 1-phenyloctane (TCI). Concentrations of the sample were varied from 1×10^{-6} M to 7×10^{-4} M in order to investigate the concentration dependent structural modulation.[13] A drop of this solution (15 μL for initial tests without annealing treatment) was applied on a freshly cleaved basal plane of a 1 cm^2 piece of highly oriented pyrolytic graphite (HOPG, grade ZYB, Momentive Performance Material Quartz Inc., Strongsville, OH). To promote the formation of the thermodynamically favored phase, annealing treatment at 80 °C for 3 h was applied. When the sample was annealed, a homemade liquid cell was employed to minimize effect of solvent evaporation by using a large amount of the sample solution (40 μL). Moreover, this liquid cell was covered with a stainless lid in an oven. The proportion of the solvent loss was estimated by weighing the liquid cell system to be 7% after annealing at 80 °C for 3 h. Then, all STM observations were performed at the liquid/graphite interface at room temperature. By changing the tunneling parameters during the STM imaging, namely, the voltage applied to the substrate and the average

tunneling current, it was possible to switch from the visualization of the adsorbate layer to that of the underlying HOPG substrate. This enabled us to correct for drift effects by the use of SPIP^{TM} software (Scanning Probe Image Processor, SPIP^{TM}, version 4.0.6 or 6.0.13, ImageMetrogyA/S, Hørsholm, Denmark). The white colored axes shown in Figures indicate the direction of main symmetry axes of graphite underneath the molecular layers. The unit cell parameters are determined from more than 30 experimental values of at least two calibrated STM images. For the statistical analysis of the surface coverage, more than 26 large area STM images (50 nm × 50 nm or larger) from two independent experimental sessions were used (Figure S3). For example, the surface coverages of the parallelogram and hexagonal B structures at concentration of 1×10^{-6} M are 2% and 78% (Figure S3a). The other area (20%) are the disordered and small domains (less than three repeating units (unit cells)).

Density Functional Theory (DFT) Simulation. All quantum chemical calculations were performed using the Gaussian 16 program package, revision A.03.[33] To estimate energy difference at a single molecular level, we performed DFT simulations of three model geometries, I-C_{3h}-*anti*, II-C_s-*syn*-1 and III-C_s-*syn*-2 geometries, of **DBA-OC14-OC1** in vacuum at the B3LYP/6-311G(d,p) level of theory. All molecules were optimized with given symmetry constraints in a closed-shell state. Vibrational frequency calculations confirmed the absence of imaginary frequencies for I-C_{3h}-*anti*. The other geometries, II-C_s-*syn*-1 and III-C_s-*syn*-2 geometries are judged as higher order saddle points because two and three imaginary frequencies were recorded. For a comparison of the thermal stability

of the regioisomers, the relative energies (E_{rel}) were calculated using the zero-point-corrected energies (ZPEs) of each isomer.

Molecular Mechanics (MM) Simulation. All MM simulations were performed with the Materials Studio 2017 R^2 using the Forcite module with COMPASS force field. The initial structures of the DBA molecules were built from the respective molecular models which were optimized by the semiempirical PM3 method. Then the orientation of the alkyl chains relative to the π system was adjusted based on that observed in the STM images. The molecules were placed 0.350 nm above the first layer of a two-layer sheet of graphene (interlayer distance is 0.335 nm), which represents graphite. This double layer graphene flake was frozen during the simulations, and a cutoff of 2.0 nm was applied for the van der Waals interactions (Lennard-Jones type). Moreover, the initial orientation of the alkyl chains relative to the π-system was adjusted to form alkyl chain interactions between the DBAs. Experimentally derived unit cells are used as periodic boundary conditions (PBC) that are summarized in Table 1.

RESULTS AND DISSCUSION

Self-Assembly of DBAs at the Liquid/Graphite Interface

At the TCB/graphite interface, **DBA-OC14-OC1** forms three monolayer structures. Figure 2a displays STM image of a monolayer formed at the lowest concentration of 3×10^{-6} M. In STM images, bright features correspond to the π-conjugated cores of the DBAs, while dark striped features connecting the DBA cores are the alkyl chains.[34] This confirms the formation of a honeycomb structure. Unit cell parameters of the honeycomb structure of **DBA-OC14-OC1** are a = b = 5.0 ± 0.1 nm and $\gamma = 60 \pm 1°$ (Table 1). The molecular packing density is 0.094 molecule·nm^{-2}. A network model optimized by MM simulation using COMPASS force field is shown in Figure 2b. Details on the MM simulation are described in the following section. Each molecule adopts a C_{3h}-symmetric geometry with the straight alkyl chains adopting an all-*anti*-configuration, similar to **DBA-OCn** with six alkyl chains, and interacts with three adjacent molecules equally via van der Waals interactions between two alkyl chains ([1+1] mode). Moreover, the alkyl chains lie parallel to the main symmetry axes of the underlying graphite surface.[35,36] Along the rim of the porous space, slightly dim dots are observed, which we attribute to co-adsorbed TCB molecules. Similar dots aligned along the inner rim are observed more clearly for **DBA-OC14-OMOM**, a synthetic intermediate of **DBA-OC14-OC1** (Figure S1).

At the intermediate concentration (6×10^{-5} M), two other structures, parallelogram and hexagonal A structures coexist, yet their surface coverage could not be determined because the domain size is

relatively small (Figure S2). The former structure contains parallelogram shaped pores (Figure 2c). Again, all alkyl chains lie parallel to the main symmetry axes of the underlying graphite surface. Unit cell parameters of this parallelogram structure are a = 2.6 ± 0.1 nm, b = 4.7 ± 0.1 nm, γ = 84 ± 2° and the molecular packing density is 0.16 molecule·nm^{-2} (Table 1). An MM optimized structure is shown in Figure 2d. It should be pointed out that, unlike the honeycomb pattern, each molecule adopts a less symmetric C_s-symmetric geometry. In this conformation, one of the alkyl chains adopts a different orientation from the other two with an apparent bending by adopting a *syn*-conformation in a butylene unit [-$(CH_2)_4$-] to maintain favorable commensurate conditions with the graphite surface and also intermolecular interactions.[35,36] Two triangular cores are located close to each other forming a pair. Between the adjacent pairs, the DBA molecules are connected via van der Waals interactions. At the long sides of the parallelogram, the two alkyl chains interact in the [1+1] mode. On the other hand, the four alkyl chains, each belonging to another DBA molecule, are involved at the short sides ([1+1+1+1] mode).

Figure 2e is an STM image of the additional structure, hexagonal A structure, which appears at the highest concentration dominantly (7 × 10^{-4} M). The six DBA molecules form a cyclic hexamer including a hexagonal pore. This unit is arranged in a hexagonal manner. All alkyl chains lie parallel to the main symmetry axes of the underlying graphite surface. Unit cell parameters of the hexagonal A structure are a = b = 6.8 ± 0.1 nm and γ = 60 ± 1° and the molecular packing density is 0.15 molecule·nm^{-2} (Table 1). An MM optimized hexagonal A structure is shown in Figure 2f. Each DBA

molecule adopts the less symmetric C_s geometry and forms a dimer similar to the one observed in the parallelogram pattern. Each molecule in the dimer unit interacts with two adjacent molecules via alkyl chain interactions ([1+1+1] mode). In all three structures, the porous areas are imaged as dim fuzzy features. We consider that the mobile solvent TCB molecules or DBA molecules are most likely co-adsorbed inside the pore.[17,27] Overall, this DBA molecule forms three structures critically depending on the solute concentration in TCB (Figure 3). It should be mentioned that Lackinger and co-workers reported similar hexagonal low and high density phases, called flower and chickenwire structures, formed by trimesic acid in different solvents.[37]

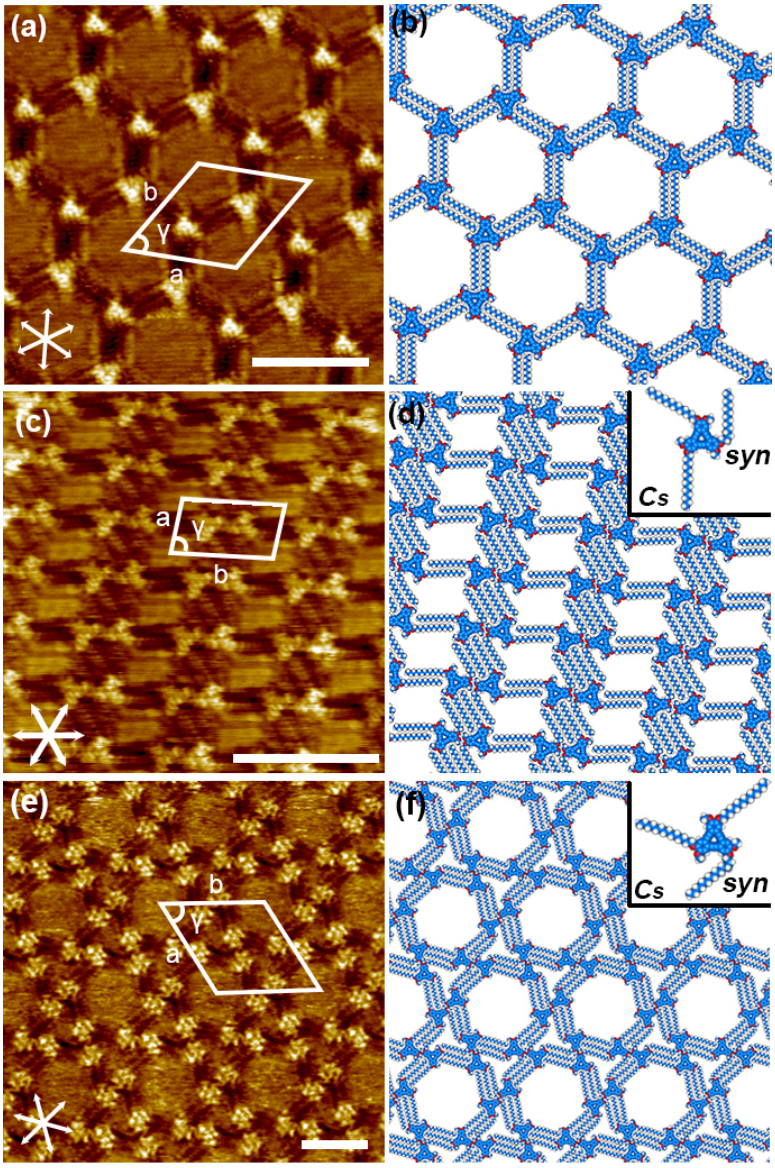

Figure 2. Monolayers formed by **DBA-OC14-OC1** at the TCB/graphite interface: STM images of (a) a honeycomb structure (3×10^{-6} M, I_{set} = 250 pA, V_{bias} = −0.35 V), (c) parallelogram structure (6×10^{-5} M, no annealing treatment yet structural features are identical to those observed after annealing, I_{set} = 100 pA, V_{bias} = −0.29 V) and (e) hexagonal A structure (7×10^{-4} M, I_{set} = 250 pA, V_{bias} = −0.75 V). Scale bars in the bottom right corner of the STM images are 5 nm. The pore diameter of the hexagonal pore, defined as the line connecting the edges of opposite triangular DBA cores, measures 4.3 ± 0.1 nm. (b, d, f) Molecular models of corresponding structures optimized by the MM simulations

with COMPASS force field. In these network models, the bilayered graphene sheets are omitted for clarity. Insets in (d, f) are geometries of a single **DBA-OC14-OC1** molecule in the networks, and "*syn*" indicates a *syn*-conformation of a butylene unit. Other parts of the adsorbed chains adopt an *anti*-conformation.

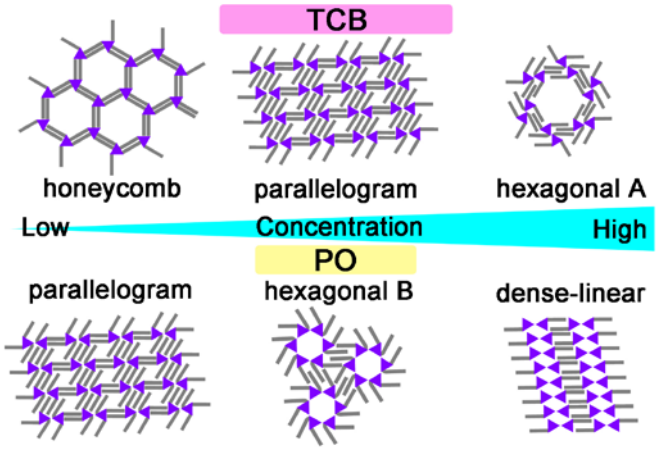

Figure 3. Overview of the concentration dependent structural variation observed for **DBA-OC14-OC1** in different solvents, TCB and PO.

The reference compound, **DBA-OC14** having six OC14 chains forms the honeycomb and linear structures upon solute concentration modulation in TCB.[13,17,23] Whereas **DBA-OC14** adopts a D_{3h}-symmetric geometry with all six alkyl chains adsorbed on the surface in the former structure (Figure 1b and 8a), it adopts a C_1 symmetric geometry with only four or five alkyl groups placed on the surface in the latter pattern; the remaining one or two orient opposite to the graphite surface and are dissolved in the solution phase (Figures 8b,c).[17,23] In both structures, the molecules are connected by

van der Waals linkages of the [2+2] type which consists of two alkyl chains of each molecule. While the honeycomb structure appears in a wide concentration range (from 10^{-6} M to 10^{-4} M), the non-porous linear structure appears at high concentration (7×10^{-4} M). In contrast, **DBA-OC14-OC1** produces the honeycomb structure only at the lowest concentration (3×10^{-6} M). At the intermediate concentration (6×10^{-5} M), new monolayer structures, the parallelogram and hexagonal A structures are formed through a combination of the alkyl chain interaction modes ([1+1], [1+1+1+1], and [1+1+1] modes). At the highest concentration (7×10^{-4} M), **DBA-OC14-OC1** forms the hexagonal A structure. Obviously, the DBA with three alkoxy chains shows a larger variety of interaction modes compared to that with six alkoxy chains. Since in the observed patterns **DBA-OC14-OC1** adopts a low symmetry C_s or C_1 geometry, the variation of the interaction modes and the resulting network patterns likely originate from the increased conformational flexibility of the alkoxy chains on surface, in combination with the reduced driving force to adopt high-symmetry geometry (C_{3h}) as required to form [1+1] type linkages, unlike **DBA-OC14**. It should be noted that the pore size of the honeycomb structure is enlarged for **DBA-OC14-OC1** because of the smaller number of interacting alkyl chains at the rims. The corner to corner distance is 4.3 ± 0.1 nm for **DBA-OC14-OC1** and 3.9 nm for **DBA-OC14**,[38] leading to a 20% pore area enlargement, yet the unit cell parameters are identical.

Next, we investigated the self-assembly of **DBA-OC14-OC1** in 1-phenyloctane (PO). Three monolayer structures are observed for **DBA-OC14-OC1**. At the lowest concentration of 1×10^{-6} M, a parallelogram structure is observed (Figure 4a). The structural features deduced from STM image

are similar to those observed in TCB. Again, each molecule adopts a less symmetric C_s-symmetric geometry. It should be noted that four PO molecules co-adsorb in the parallelogram pore (Figure S4). Occasionally, a bright feature is observed in the pore (indicated by green arrow in Figure 4a). We attribute this to a DBA molecule adopting a compact conformation for its alkyl chains.[39] The unit cell parameters are a = 2.7 ± 0.1 nm, b = 4.4 ± 0.1 nm, and γ = 84 ± 1° and are slightly different to those in TCB. A network model based on MM optimization is shown in Figure 4b. Moreover, another structure, a hexagonal B structure coexists, in which a cyclic hexamer is arranged in a hexagonal manner forming a small hexagonal pore (Figure 4c). One of the alkyl chains is not observed on the surface and orients to the solution phase. The DBA molecule adopts a C_1 conformation as one of the alkyl chains is not adsorbed on the surface. At each hexagonal vertex, the four alkyl chains, each belonging to individual four DBA molecules, are involved in intermolecular interactions ([1+1+1+1] mode). These alkyl chains run parallel to the main symmetry axes of graphite. An MM optimized network model is displayed in Figure 4d. Fuzzy linear features between the hexamer units can be attributed to PO molecules co-adsorbed in the space formed by the alkyl chains (Figure S5). Unit cell parameters of this hexagonal B structure are a = b = 5.6 ± 0.1 nm, γ = 60 ± 1° and the molecular packing density is relatively high (0.22 molecule·nm^{-2}, Table 1). Surface coverages of the parallelogram and hexagonal B structures at this concentration are 2% and 78% (Figures S3a,c).

At higher concentration (5×10^{-5} M), in addition to the hexagonal B structure, a dense-linear structure is observed (Figure 4e). Two alkyl chains per molecule are not observed and orient to the

solution phase. Each DBA molecule adopts a C_1 geometry. The DBA molecules align linearly to form double molecular rows. These rows are connected via two alkyl chains between the DBAs ([1+1] mode). These adsorbed alkyl chains are aligned parallel to the main symmetry axes of graphite. An MM optimized network structure is shown in Figure 4f. The solvent PO molecules are co-adsorbed in the space between the alkyl chains of the DBAs (Figure S6). Unit cell parameters of this structure are a = 1.4 ± 0.1 nm, b = 4.4 ± 0.1 nm, γ = 84 ± 1° and the molecular packing density is very high (0.34 molecule·nm^{-2}, Table 1). Surface coverages of the dense-linear and hexagonal B structures at this concentration are 36% and 38% (Figures S3b,d).

In conclusion, in PO, **DBA-OC14-OC1** also forms three structures (Figure 3). However, no honeycomb structure appears even at the lowest concentration studied, in contrast to the reference compound **DBA-OC14**.[40] Two new structures show a variety of the alkyl chain interaction modes, as observed for the self-assemblies in TCB (vide supra).

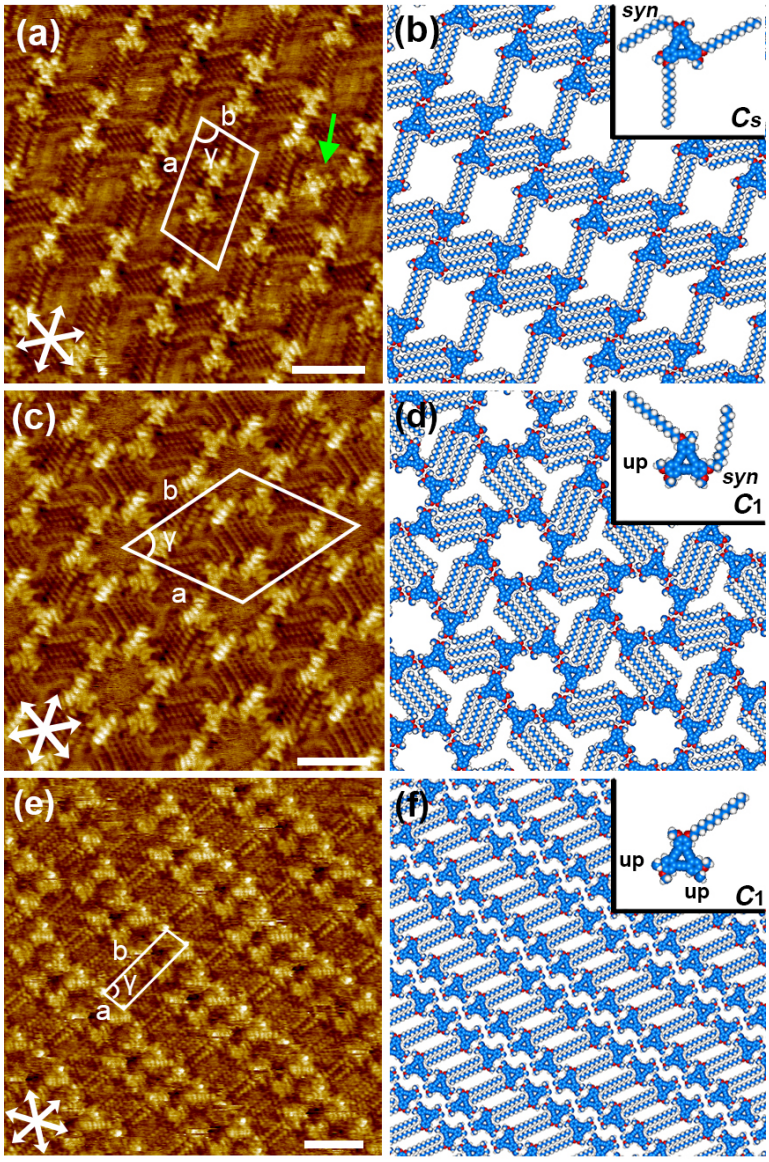

Figure 4. Monolayers formed by **DBA-OC14-OC1** at the PO/graphite interface: STM images of (a) parallelogram (1×10^{-6} M, I_{set} = 350 pA, V_{bias} = −0.31 V), (c) hexagonal B (1×10^{-6} M, I_{set} = 350 pA, V_{bias} = −0.31 V) and (e) dense-linear structures (5×10^{-5} M, I_{set} = 100 pA, V_{bias} = −0.35 V). Green arrow in (a) indicates a bright parallelogram pore, likely corresponding to a co-adsorbed DBA molecule. Scale bars in the bottom right corner of the STM images are 3 nm. Molecular models of (b) parallelogram, (d) hexagonal B and (f) dense-linear structures optimized by the MM calculations with COMPASS force field. In these network models, the alkoxy chains which orient to the solution

phase (one and two chains per DBA molecule for the hexagonal B and dense-linear structures, respectively) are replaced by a methyl group and bilayered graphene sheets are omitted for clarity. Insets in (b, d, f) are geometries of a single **DBA-OC14-OC1** molecule in the networks, and "*syn*" and "up" indicates butylene units having *syn*-conformation and non-adsorbed alkyl chains, respectively. Other parts of the adsorbed chains adopt an *anti*-conformation.

Table 1. Experimentally Derived Unit Cell Parameters, Unit Cell Area, Number of Molecules in the Unit Cell and Surface Molecular Densities for Molecular Networks Formed by **DBA-OC14-OC1** at the Liquid/Graphite Interfaces.

solvent	structure	a (nm)	b (nm)	γ (°)	area (nm^2)	number of DBA molecules	surface molecular density (molecule·nm^{-2})[a]
TCB	honeycomb structure	5.0 ± 0.1		60 ± 1	20.9	2	0.094
	parallelogram structure	2.6 ± 0.1	4.7 ± 0.1	84 ± 2	12.2	2	0.16
	hexagonal A structure	6.8 ± 0.1		60 ± 1	40.0	6	0.15
PO	parallelogram structure	2.7 ± 0.1	4.4 ± 0.1	84 ± 1	11.5	2	0.17
	hexagonal B structure	5.6 ± 0.1		60 ± 1	26.8	6	0.22
	dense-linear structure	1.4 ± 0.1	4.4 ± 0.1	84 ± 1	6.0	2	0.34

[a] Number of the DBA molecules per unit area.

Conformational Flexibility of Alkyl Chains of DBA-OC14-OC1 at Single Molecule Level

The observed structural variation of **DBA-OC14-OC1** likely originates from its conformational flexibility on surface compared to **DBA-OC14**. To estimate the energy difference at the single molecule level, we performed DFT calculations of three model geometries, I-C_{3h}-*anti*, II-C_s-*syn*-1 and III-C_s-*syn*-2 geometries, of **DBA-OC14-OC1** in vacuum at the B3LYP/6-311G(d,p) level of theory (Figure 5). All OC14 chains of the geometry I have *anti*-conformation. In the geometries II and III, one butylene unit adopts a *syn*-conformation in the bent chain. The difference between the geometries II and III is the orientation of the methyl group attached to the same benzene ring to which the bent butylene unit is attached. The geometry I is the most stable, equilibrium structure in vacuum (Figure 5). For the other geometries II and III, two and three imaginary frequencies are recorded, indicating that these are on higher order saddle points. The energies relative to that of the geometry I are 5.5 kcal·mol^{-1} for the geometry II-C_s-*syn*-1 and 8.2 kcal·mol^{-1} for the geometry III-C_s-*syn*-2 and could be easily compensated by intermolecular and molecule-substrate interactions at the surface.[41] This indicates that the II-C_s-*syn*-1 is the most suitable candidate of the geometry for the construction of the parallelogram, and hexagonal A and B structures. Obviously, one OC14 chain of **DBA-OC14** could not adopt such bent conformation because of the steric repulsion with the adjacent chain. Moreover, the energy penalty for the rotation of the methyl groups of **DBA-OC14-OC1** is only 2.7 kcal·mol^{-1} (II vs. III). These calculations support that the OC14 chains and methoxy groups of **DBA-OC14-OC1** have enhanced conformational freedom.

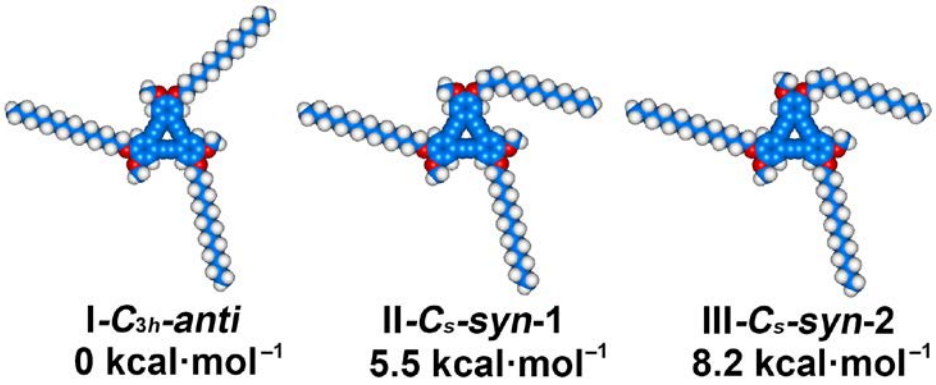

Figure 5. DFT optimized geometries, I-C_{3h}-*anti*, II-C_s-*syn*-1 and III-C_s-*syn*-2 of a single **DBA-OC14-OC1** molecule with relative energies with respect to the most stable geometry I under vacuum.

Energies Estimated by MM Simulations

To gain further insight into the factors that influence polymorph formation, interaction energies are analyzed by MM simulations. Experimentally derived unit cell parameters summarized in Table 1 are used as periodic boundary conditions (PBC). In the modeling of network structures in PO, co-adsorbed solvent molecules are included according to the STM image analyses (Figures S4–S6). For the hexagonal B structure, we modeled two structures with different numbers of co-adsorbed PO molecules (two or five molecules). In the case of TCB, we assume that the pore spaces are occupied by the maximum numbers of TCB molecules.[17,27,42] In addition to the **DBA-OC14-OC1** networks, the models of the honeycomb and linear structures of **DBA-OC14** are optimized for comparison, and starting geometries are built according to previous reports.[13,17,23] Figures 6–8 show optimized geometries of the six observed structures of **DBA-OC14-OC1** and the two structures of **DBA-OC14**. Table 2 summarizes estimated energies per unit area to compare the relative stability of the monolayer networks. Here we use "*e*" and "Δ*h*" for calculated energy and enthalpy, respectively, instead of *E* and Δ*H* according to the convention adopted by Gulzler *et al*.[43] The Δh_{DBA} and Δh_{solv} values are enthalpy changes upon adsorption of a single DBA molecule and solvent molecules for the respective networks. The Δ*h* values are the sum of the Δh_{DBA} and Δh_{solv} values. Details of the MM simulations and energy calculations are described in Supporting Information. Note that however this approach estimates only partial enthalpy changes in the network formation at the interface as the solvent layer

is ignored. The solvation energies for the DBA molecule in the solution phase and wetting energies for the network are not considered.[44,45]

First, we evaluate relative stabilities of three structures formed by **DBA-OC14-OC1** in TCB. The Δh_{DBA} values of the pristine honeycomb, parallelogram, and hexagonal A structures are –15.3, –26.5 and –22.7 kcal·mol^{-1}·nm^{-2}, respectively. The least negative Δh_{DBA} value for the honeycomb structure is attributed to a low surface molecular density. Because the pore size and shape are different between three structures, the contribution of the co-adsorbed solvent molecules, Δh_{solv}, also varies as –27.2, –12.9, and –16.4 kcal·mol^{-1}·nm^{-2} for the honeycomb, parallelogram, and hexagonal A structures. As a result, Δh becomes –42.5, –39.4, and –39.1 kcal·mol^{-1}·nm^{-2} for the honeycomb, parallelogram, and hexagonal A structures, respectively. We consider that the small differences in the Δh values relate to the appearance of the three structures upon changing the concentration~~, yet the present Δh values do not include a solvation energy~~. Similar analyses on the **DBA-OC14** networks show that the Δh values of the honeycomb and linear structures are –44.2 kcal·mol^{-1}·nm^{-2} and –39.3 for the pristine networks, respectively, and –41.9 kcal·mol^{-1}·nm^{-2} for the linear network with co-adsorbed TCB molecule. This energy difference, in particular between the honeycomb and linear structure without the co-adsorbed TCB molecule is in accord with the favorable formation of the honeycomb structure in a wide concentration range for **DBA-OC14**.[13]

To see the effect of removal of three alkyl chains on the relative stability of the molecular networks, the energy values of the honeycomb structures of **DBA-OC14-OC1** and **DBA-OC14**, in which the

surface molecular densities are identical, are compared. Obviously, the Δh_{DBA} of **DBA-OC14-OC1** is larger than that of **DBA-OC14** because of the smaller number of alkyl chains (–15.3 and –25.4 kcal·mol^{-1}·nm^{-2} for **DBA-OC14-OC1** and **DBA-OC14**) which contribute significantly to $e_{mol\text{-}sub}$ (–13.7 and –21.6 kcal·mol^{-1}·nm^{-2}, respectively). On the other hand, the contribution of the solvent molecules is significant for **DBA-OC14-OC1** due to the larger number of co-adsorbed TCB molecules. Namely, the Δh_{solv} values are –27.2 and –18.8 kcal·mol^{-1}·nm^{-2} for **DBA-OC14-OC1** and **DBA-OC14**, respectively. Overall, the Δh value of the **DBA-OC14** honeycomb structure is smaller than that of **DBA-OC14-OC1**, suggesting that the molecular network of the former with [2+2] linkages is more stable in spite of the smaller contribution of solvent co-adsorption.

Next, the relative stabilities of three polymorphs of **DBA-OC14-OC1** in PO are compared. The Δh_{DBA} values of the parallelogram, hexagonal B, and dense-linear structures observed in PO are –28.4, –31.1, and –37.7 kcal·mol^{-1}·nm^{-2}, respectively. The values for the hexagonal B and dense-linear structures are small compared to that of the parallelogram structure because of the higher surface molecular packing densities. On the contrary, the Δh_{solv} value is the smallest for the parallelogram structure. The Δh values of the parallelogram, hexagonal B, and dense-linear structures are –40.9, –36.5 (or –34.0), and –42.5 kcal·mol^{-1}·nm^{-2}, respectively. The hexagonal B structure is estimated to be the least stable among the structures, in contrast to the experimental observations where it appears in the wide concentration range. This result may originate from the difficulty in treating the unresolved porous area, where the six alkoxy chains of the DBAs and/or solvent molecules could be

adsorbed (Figures 7c,d). Co-adsorption of the alkyl fragments or solvent molecules would bring enthalpic gains and the dissolvation of alkyl chains would lead to entropic gains, contributing to further stabilization of the hexagonal B structure (vide infra).

Estimate of Entropy Change by Desorption of DBA Molecule from Networks

To address the entropic contribution to the observed structural variation, a very rough estimate of the entropic gain ($T\Delta S_{297}$) upon desorption of a single DBA molecule from the solution phase was performed according to the Whitesides's approach (See Supporting Information).[17,44,46,47] The estimated entropy gain varies depending on the number of solvated alkyl chains per single **DBA-OC14-OC1** molecule in the respective network at the single molecular level (Tables S9 and S10). For instance, it becomes the largest for the parallelogram structure with three adsorbed chains (54.4 kcal·mol^{-1}), while the smallest for the dense linear structure with only one adsorbed chain (38.3 kcal·mol^{-1}). In contrast, when the entropy gain is expressed per unit area, it becomes the smallest for the parallelogram structure (9.4 kcal·mol^{-1}·nm^{-2}) and the largest for the dense linear structure (12.7 kcal·mol^{-1}·nm^{-2}). This indicates that molecular density influences the total entropy gain of the system, *i.e.* low density network formation is favored over high density network formation, yet the energy difference is not so large. Moreover, the $T\Delta S_{297}$ values by desorption of a single **DBA-OC14** or **DBA-OC14-OC1** molecule from the honeycomb structures reveal that adsorption of **DBA-OC14** is entropically less favorable compared to **DBA-OC14-OC1** (Table S9 and S11).

It should be mentioned however that the present method does not take the difference in the number of adsorbed molecules on the surface and released molecules in the solution phase into account, which also affect the total entropy changes of the system. This is expected to be important at the level of the DBA molecule, in particular at low solute concentrations. Detailed and quantitative insight into the role entropy plays will require further study.

Effect of Solvent Co-Adsorption: 1,2,4-Trichlorobenzene vs. 1-Phenyloctane

The distinct difference in the monolayer structures between the two solvents is the surface molecular density. More specifically, the structures in PO (0.17–0.34 molecules·nm^{-2}) are denser compared with those in TCB (0.094–0.16 molecules·nm^{-2}). More solvent molecules are co-adsorbed within the networks in the case of TCB. [49] A similar trend was previously reported for the monolayers formed by the DBA molecules having six alkoxy chains.[23] We compare the effect of the solvents for the parallelogram structures that are formed in both solvents. The Δh_{DBA} and Δh_{solv} values are similar. At the parallelogram pores, six TCB molecules and four PO molecules could be accommodated taking the size and shape complementarity into account. However, the enthalpic gains by the solvent co-adsorption per a unit area are comparable between TCB and PO. The question arises why the low density networks are favored in TCB, yet the enthalpic gains are comparable. To address the entropic gain upon desorption of the solvent molecules, we performed a very rough estimation of the entropic changes ($T\Delta S_{297}$) upon desorption of a solvent molecule from graphite surface according to the

Whitesides's approach, which afforded 13.7 kcal·mol^{-1} for TCB and 19.7 kcal·mol^{-1} for PO (See Supporting Information). [17,44,46,47] Though the desorption of PO is favored at the single molecule level compared to TCB, it becomes comparable per unit area when the number of solvent molecules is taken into account (4 vs. 6 for PO and TCB in the pore, respectively). As such, we do not have a clear answer at this moment. The reason could relate to factors that are not considered in the present study. For example, we did not consider the solvation energies of the DBA molecule which must be different for PO and TCB.

Table 2. Calculated Energies and Enthalpies per Unit Area (kcal·mol^{-1}·nm^{-2}) of Self-Assembled Molecular Networks Formed by **DBA-OC14-OC1** and **DBA-OC14**.

			number of solvent molecules included per PBC	$\Delta e_{\text{mol-sub}}$[a]	$\Delta e_{\text{mol-mol}}$[b]	Δh_{DBA}[c]	Δh_{solv}[d]	Δh[e]
DBA-OC14-OC1	TCB	honeycomb structure	23	−13.7	−1.6	−15.3	−27.2	−42.5
		parallelogram structure	6	−24.4	−2.1	−26.5	−12.9	−39.4
		hexagonal A structure	26	−21.6	−1.1	−22.7	−16.4	−39.1
	PO	parallelogram structure	4	−25.8	−2.6	−28.4	−12.5	−40.9
		hexagonal B structure	2	−29.2	−1.9	−31.1	−2.9	−34.0
			5	−27.9	−0.7	−28.6	−7.9	−36.5
		dense-linear structure	1	−33.2	−4.5	−37.7	−4.8	−42.5
DBA-OC14	TCB	honeycomb structure	16	−21.6	−3.8	−25.4	−18.8	− 44.2
		linear structure	0	−32.9	−6.4	−39.3	0	− 39.3
			1	−32.9	−6.4	−39.3	–2.6	− 41.9

[a]Interaction energies with the substrate upon the adsorption of a single DBA molecule ($\Delta e_{\text{mol-sub}}$) in each network. [b]Intermolecular interactions upon adsorption of a single DBA molecule ($\Delta e_{\text{mol-mol}}$) in each network. This does not include the interactions between the solvent and DBA molecules. [c]Enthalpy change upon adsorption of a single DBA molecule in each network ($\Delta e_{\text{mol-sub}} + \Delta e_{\text{mol-mol}}$). [d]Enthalpy change upon co-adsorption of the solvent molecules in each network. [e]Total enthalpy change in each network ($\Delta h_{\text{DBA}} + \Delta h_{\text{solv}}$). This does not include solvation energies. Details are described in Supporting Information.

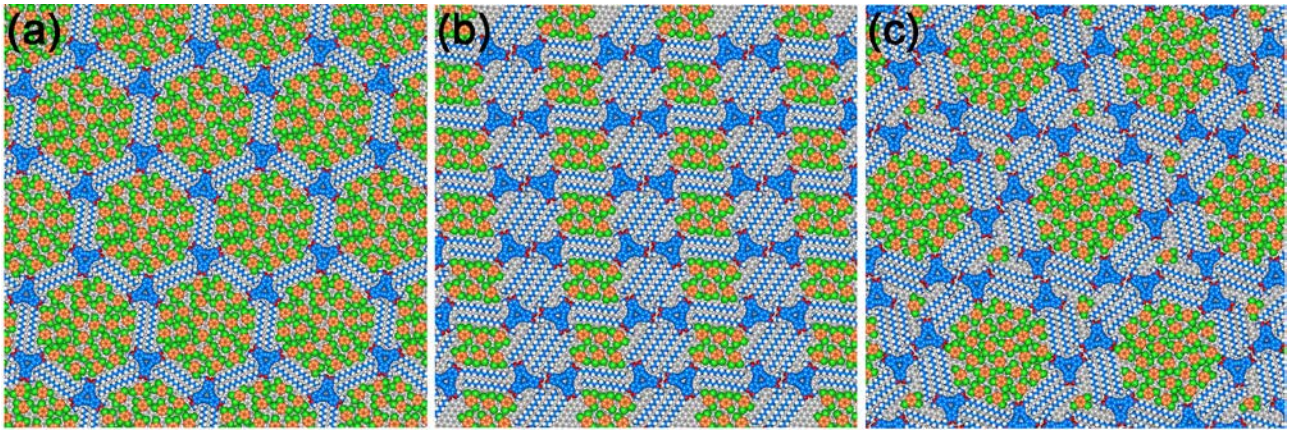

Figure 6. MM optimized molecular models of (a) honeycomb structure with 23 co-adsorbed TCB molecules, (b) parallelogram structure with six co-adsorbed TCB molecules, and (c) hexagonal A structure with 26 co-adsorbed TCB molecules. Numbers of co-adsorbed TCB molecules are per PBC. Carbon atoms of **DBA-OC14-OC1** and TCB molecules, and graphene sheets are shown in blue and orange, and gray, respectively.

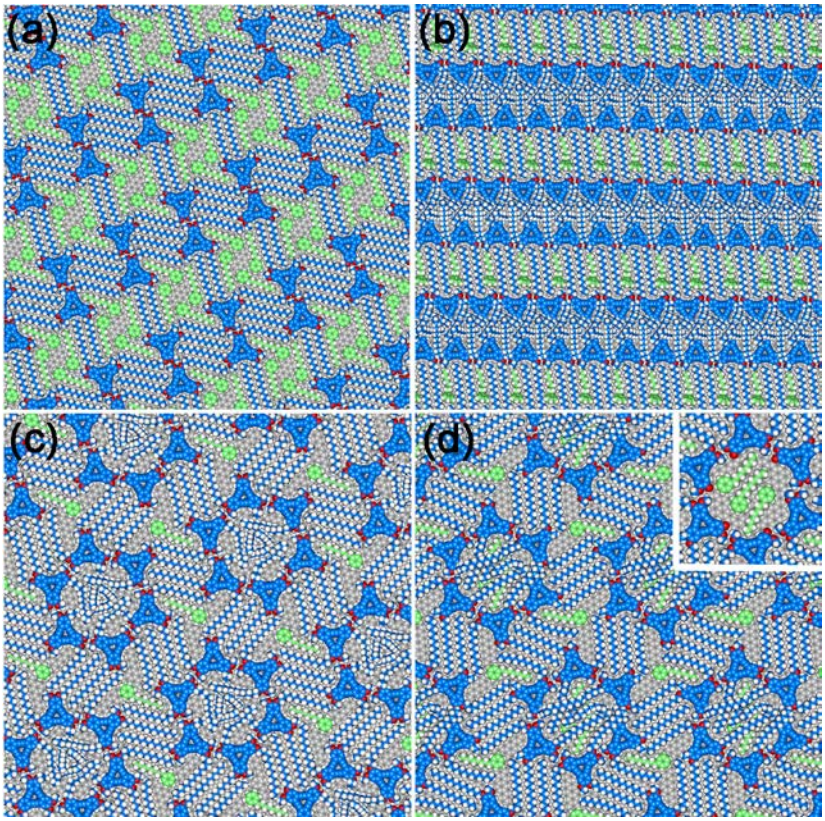

Figure 7. MM optimized molecular models of (a) parallelogram structure with four co-adsorbed PO molecules, (b) dense-linear structure with one PO molecule, and (c, d) hexagonal B structure with two or five PO molecules. Inset in image (d) is pore where the alkyl chains orienting to the solution phase are omitted. Numbers of co-adsorbed PO molecules are per PBC. Carbon atoms of **DBA-OC14-OC1** and PO molecules, and graphene sheets are shown in blue and light green, and gray, respectively.

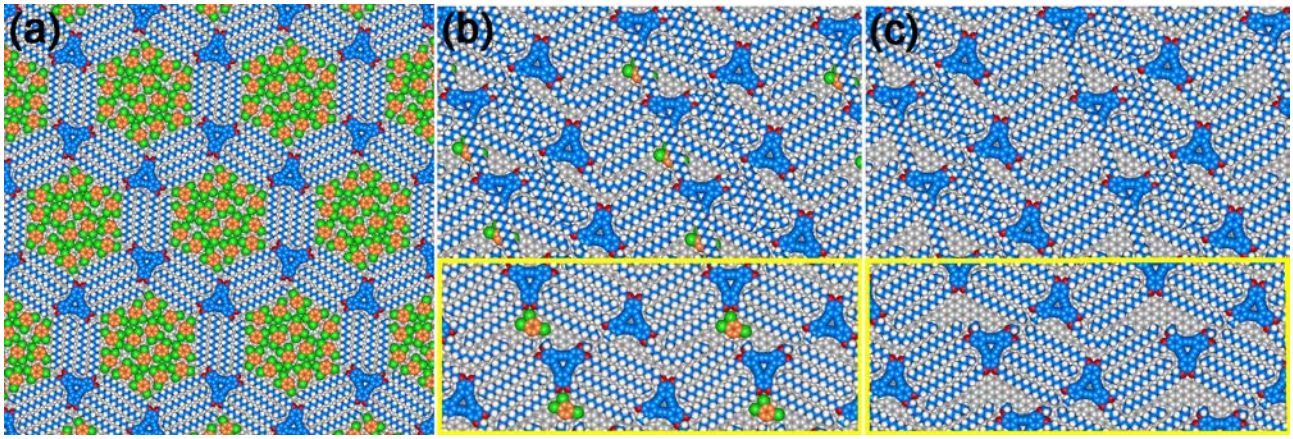

Figure 8. MM optimized molecular models of (a) a honeycomb structure of **DBA-OC14** with 16 co-adsorbed TCB molecules, (b, c) a linear structure of **DBA-OC14** with one (b) or no (c) co-adsorbed TCB molecule. In yellow boxes at the bottom of (b, c), one or two non-adsorbed alkyl chain(s) of single **DBA-OC14** molecule is/are replaced with methyl group(s) for clarity. In the linear structure, **DBA-OC14** adopts two molecular geometries: one with four adsorbed alkyl chains and the other with five adsorbed alkyl chains. One adsorbed chain in the later geometry adopts a bent formation, while the other adsorbed chains form [2+2] type linkages. Carbon atoms of **DBA-OC14** and TCB molecules, and graphene sheets are shown in blue and orange, and gray, respectively.

CONCLUSION

A new DBA derivative **DBA-OC14-OC1** having three long tetradecyloxy chains and three methoxy groups was synthesized to investigate the impact of the number of alkyl chains on 2D self-assembly at the TCB or PO/graphite interface. The structural patterns were compared with those formed by **DBA-OC14** with six tetradecyloxy chains. STM observations revealed the formation of a variety of self-assembled structures of **DBA-OC14-OC1** in both solvents. In TCB, it forms the porous honeycomb, parallelogram, and hexagonal A structures. The hexagonal pore size area is enlarged by ca. 20% compared to **DBA-OC14**. Moreover, three structures, parallelogram, hexagonal B and dense-linear structures were observed in PO. In contrast to **DBA-OC14** which adopts [2+2] alkyl chain interaction mode, **DBA-OC14-OC1** adopts a variety of interaction modes ([1+1], [1+1+1], and [1+1+1+1] modes) consisting of one alkyl chain per molecule. Since the observed patterns of **DBA-OC14-OC1** show a low symmetric C_s or C_1 geometry for this DBA derivative, the variation of the interaction modes and the resulting network patterns likely originate from the on-surface conformational flexibility of the alkoxy chains, made possible by their decrease in number. Therefore, there is no driving force for **DBA-OC14-OC1** to adopt high-symmetry geometry (C_{3h}) required to form [1+1] type linkages, unlike **DBA-OC14**. MM simulations address the energy aspects of these structures. The relatively small enthalpy differences between the structures are in line with the experimentally observed polymorphism. We also discussed solvent co-adsorption to shed light on the different trends in PO and TCB. The fact that **DBA-OC14-OC1**, counting only three long alkoxy

groups instead of six, under certain conditions forms a honeycomb structure is promising for the future formation of functionalized pores. Indeed, we conceive that pore functionalization will be possible simply by introducing functional groups where now the three methoxy groups are located. This will expand our design strategy for the production of tailored functional surfaces as well as two-dimensional polymers.

Present study provides useful information for structural control of self-assembled systems formed by trigonal building block, thereby illustrating the strong impact of the number of alkyl chains, which is of importance in the field of 2D crystal engineering.

ACKNOWLEDGMENT

This work was supported by JSPS KAKENHI Grant Numbers JP15H02164 and JP17K19130, the Fund of Scientific Research Flanders (FWO), and KU Leuven - Internal Funds.

SUPPORTING INFORMATION

The Supporting Information is available free of charge on the ACS Publications website.

Experimental Details, Additional STM Images, Details of MM Simulations, Energy Estimations, Characterization Data of New Compound.

INFORMATION DESCRIPTION

Corresponding Authors

*tahara@meiji.ac.jp

*steven.defeyter@kuleuven.be

*tobe@chem.es.osaka-u.ac.jp

ORCID

Kazukuni Tahara: 0000-0002-3634-541X

Steven De Feyter: 0000-0002-0909-9292

Yoshito Tobe: 0000-0002-1795-5829

Note

The authors declare no competing financial interest.

REFERENCES

(1) Goronzy, D. P.; Ebrahimi, M.; Rosei, F.; Arramel; Fang, Y.; De Feyter, S.; Tait, S. L.; Wang, C.; Beton, P. H.; Wee, A. T. S.; Weiss, P. S.; Perepichka, D. F. Supramolecular Assemblies on Surfaces: Nanopatterning, Functionality, and Reactivity. *ACS Nano* **2018**, *12*, 7445–7481.

(2) Barth, J. V.; Costantini, G.; Kern, K. Engineering Atomic and Molecular Nanostructures at Surfaces. *Nature* **2005**, *437*, 671–679.

(3) Palma, C.-A.; Samorì, P. Blueprinting Macromolecular Electronics. *Nat. Chem.* **2011**, *3*, 431–436.

(4) Ortega Lorenzo, M.; Baddeley, C. J.; Muryn, C.; Raval, R. Extended Surface Chirality from Supramolecular Assemblies of Adsorbed Chiral Molecules. *Nature* **2000**, *404*, 376–379.

(5) Barth, J. V. Molecular Architectonics on Metal Surfaces. *Annu. Rev. Phys. Chem.* **2007**, *58*, 375–407.

(6) Elemans, J. A. A. W.; Shengbin, L.; De Feyter, S. Molecular and Supramolecular Networks on Surfaces: From Two-Dimensional Crystal Engineering to Reactivity. *Angew. Chem. Int. Ed.* **2009**, *48*, 7298–7332.

(7) Theobald, J. A.; Oxtoby, N. S.; Phillips, M. A.; Champness, N. R.; Beton, P. H. Controlling Molecular Deposition and Layer Structure with Supramolecular Surface Assemblies. *Nature* **2003**, *424*, 1029–1031.

(8) Rabe, J. P.; Buchholz, S. Commensurability and Mobility in Two-Dimensional Molecular Patterns on Graphite. *Science* **1991**, *253*, 424–427.

(9) Furukawa S., De Feyter S. Two-Dimensional Crystal Engineering at the Liquid–Solid Interface. In: Broekmann P., Dötz KH., Schalley C.A. (Eds) Templates in Chemistry III. Topics in Current Chemistry, vol 287. Springer, Berlin, Heidelberg (2008).

(10) Plass, K. E.; Grzesiak, A. L.; Matzger, A. J. Molecular Packing and Symmetry of Two-Dimensional Crystals. *Acc Chem. Res.* **2007**, *40*, 287–293.

(11) Yang, Y.; Wang, C. Solvent Effects on Two-Dimensional Molecular Self-Assemblies Investigated by Using Scanning Tunneling Microscopy. *Curr. Opin. Colloid Interface Sci.* **2009**, *14*, 135–147.

(12) Miao, X.; Xu, L.; Li, Z.; Deng, W. Solvent-Induced Structural Transitions of a 1,3,5-Tris(10-ethoxycarbonyldecyloxy)benzene Assembly Revealed by Scanning Tunneling Microscopy. *J. Phys. Chem. C* **2011**, *115*, 3358–3367.

(13) Lei, S.; Tahara, K.; De Schryver, F. C.; Van der Auweraer, M.; Tobe, Y.; De Feyter, S. One Building Block, Two Different Supramolecular Surface-Confined Patterns: Concentration in Control at the Solid–Liquid Interface. *Angew. Chem. Int. Ed.* **2008**, *47*, 2964–2968.

(14) Kampschulte, L.; Werblowsky, T. L.; Kishore, R. S. K.; Schmittel, M.; Heckl, W. M.; Lackinger, M. Thermodynamical Equilibrium of Binary Supramolecular Networks at the Liquid-Solid Interface. *J. Am. Chem. Soc.* **2008**, *130*, 8502–8507.

(15) Shen, Y.-T.; Zhu, N.; Zhang, X.-M.; Deng, K.; Feng, W.; Yan, Q.; Lei, S.; Zhao, D.; Zeng, Q.-D.: Wang, C. A Foldamer at the Liquid/Graphite Interface: The Effect of Interfacial Interactions, Solvent, Concentration, and Temperature. *Chem. Eur. J.* **2011**, *17*, 7061–7068.

(16) Ciesielski, A.; Szabelski, P. J.; Rżysko, W.; Cadeddu, A.; Cook, T. R.; Stang, P. J.; Samorì, P. Concentration-Dependent Supramolecular Engineering of Hydrogen-Bonded Nanostructures at Surfaces: Predicting Self-Assembly in 2D. *J. Am. Chem. Soc.* **2013**, *135*, 6942–6950.

(17) Blunt, M. O.; Adisoejoso, J.; Tahara, K.; Katayama, K.; Van der Auweraer, M.; Tobe, Y.; De Feyter, S. Temperature-Induced Structural Phase Transitions in a Two-Dimensional Self-Assembled Network. *J. Am. Chem. Soc.* **2013**, *135*, 12068–12075.

(18) Bellec, A.; Arrigoni, C.; Schull, G.; Douillard, L.; Fiorini-Debuisschert, C.; Mathevet, F.; Kreher, D.; Attias, A.-J.; Charra, F. Solution-Growth Kinetics and Thermodynamics of Nanoporous Self-Assembled Molecular Monolayers. *J. Chem. Phys.* **2011**, *134*, 124702.

(19) Lei, S.-B.; Deng, K.; Yang, Y.-L.; Zeng, Q.-D.; Wang, C.; Jiang, J.-Z. Electric Driven Molecular Switching of Asymmetric Tris(phtalocyaninato)Lutetium Triple-Decker Complex at the Liquid/Solid Interface. *Nano Lett.* **2008**, *8*, 1836–1843.

(20) Mali, K. S.; Wu, D.; Feng, X.; Müllen, K.; Van der Auweraer, M.; De Feyer, S. Scanning Tunneling Microscopy-Induced Reversible Phase Transformation in the Two-Dimensional Crystal of a Positively Charged Discotic Polycyclic Aromatic Hydrocarbon. *J. Am. Chem. Soc.* **2011**, *133*, 5686–5688.

(21) Tahara, K.; Lei, S.; Adisoejoso, J.; De Feyter, S.; Tobe, Y. Supramolecular Surface-Confined Architectures Created by Self-Assembly of Triangular Phenylene-Ethynylene Macrocycles via van der Waals Interaction. *Chem. Commun.* **2010**, *46*, 8507–8525.

(22) Tobe, Y.; Tahara, K.; De Feyter, S. Adaptive Building Blocks Consisting of Rigid Triangular Core and Flexible Alkoxy Chains for Self-Assembly at Liquid/Solid Interfaces. *Bull. Chem. Soc. Jpn.* **2016**, *89*, 1277–1306.

(23) Tahara, K.; Furukawa, S.; Uji-i, H.; Uchino, T.; Ichikawa, T.; Zhang, J.; Mamdouh, W.; Sonoda, M.; De Schryver, F. C.; De Feyter, S.; Tobe, Y. Two-Dimensional Porous Molecular Networks of Dehydrobenzo[12]annulene Derivatives via Alkyl Chain Interdigitation. *J. Am. Chem. Soc.* **2006**, *128*, 16613–16625

(24) Tahara, K.; Kaneko, K.; Katayama, K.; Itano, S.; Nguyen, C. H.; Amorim, D. D. D.; De Feyter, S.; Tobe, Y. Formation of Multicomponent Star Structures at the Liquid/Solid Interface. *Langmuir* **2015**, *31*, 7032–7040.

(25) Tahara, K.; Johnson II, C. A.; Fujita, T.; Sonoda, M.; De Schryver, F. C.; De Feyter, S.; Haley, M. M.; Tobe, Y. Synthesis of Dehydrobenzo[18]annulene Derivatives and Formation of Self-Assembled Monolayers: Implication of Core Size on Alkyl Chain Interdigitation. *Langmuir* **2007**, *23*, 10190–10197.

(26) Velpula, G.; Takeda, T.; Adisoejoso, J.; Inukai, K.; Tahara, K.; Mali, K. S.; Tobe, Y.; De Feyter, S. On the Formation of Concentric 2D Multicomponent Assemblies at the Solution-Solid Interface. *Chem. Commun.* **2017**, *53*, 1108–1111.

(27) Tahara, K.; Okuhata, S.; Adisoejoso, J.; Lei, S.; Fujita, T.; De Feyter, S.; Tobe, Y. 2D Networks of Rhombic-Shaped Fused Dehydrobenzo[12]annulenes: Structural Variations under Concentration Control. *J. Am. Chem. Soc.* **2009**, *131*, 17583–17590.

(28) Mamdouh, W.; Uji-i, H.; Ladislaw, J. S.; Dulcey, A. E.; Percec, V.; De Schryver, F. C.; De Feyter, S. Solvent Controlled Self-Assembly at the Liquid-Solid Interface Revealed by STM. *J. Am. Chem. Soc.* **2006**, *128*, 317–325.

(29) Shen, X.; Wei, X.; Tan, P.; Yu, Y.; Yang, B.; Gong, Z.; Zhang, H.; Lin, H.; Li, Y.; Li, Q.; Xie, Y.; Chi, L. Concentration-Controlled Reversible Phase Transitions in Self-Assembled Monolayers on HOPG Surfaces. *Small* **2015**, *11*, 2284–2290.

(30) Feng, X.; Pisula, W.; Ai, M.; Gröper, S.; Rabe, J. P.; Müllen, K. Unusual Symmetry Effect on Hexa-*peri*-hexabenzocoronene. *Chem. Mater.* **2008**, *20*, 1191–1193.

(31) Lee, S.; Hirsch, B. E.; Liu, Y.; Dobscha, J. R.; Burke, D. W.; Tait, S. L.; Flood, A. H. Multifunctional Tricarbazolo Trianzolophane Macrocycles: One-Pot Preparation, Anion Binding, and Hierarchical Self-Organization of Multilayers. *Chem. Eur. J.* **2016**, *22*, 560–569.

(32) Tahara, K.; Adisoejoso, J.; Inukai, K.; Lei, S.; Noguchi, A.; Li, B.; Vanderlinden, W.; De Feyter, S.; Tobe, Y. Harnessing by a Diacetylene Unit: a Molecular Design for Porous Two-Dimensional Network Formation at the Liquid/Solid Interface. *Chem. Commun.* **2014**, *50*, 2831–2833.

(33) Frisch, M. J.; Trucks, G. W.; Schlegel, H. B.; Scuseria, G. E.; Robb, M. A.; Cheeseman, J. R.; Scalmani, G.; Barone, V.; Petersson, G. A.; Nakatsuji, H.; Li, X.; Caricato, M.; Marenich, A. V.; Bloino, J.; Janesko, B. G.; Gomperts, R.; Mennucci, B.; Hratchian, H. P.; Ortiz, J. V.; Izmaylov, A. F.; Sonnenberg, J. L.; Williams-Young, D.; Ding, F.; Lipparini, F.; Egidi, F.; Goings, J.; Peng, B.; Petrone, A.; Henderson, T.; Ranasinghe, D.; Zakrzewski, V. G.; Gao, J.; Rega, N.; Zheng, G.; Liang, W.; Hada, M.; Ehara, M.; Toyota, K.; Fukuda, R.; Hasegawa, J.; Ishida, M.; Nakajima, T.; Honda, Y.; Kitao, O.; Nakai, H.; Vreven, T.; Throssell, K.; Montgomery, J. A., Jr.; Peralta, J. E.; Ogliaro, F.;

Bearpark, M. J.; Heyd, J. J.; Brothers, E. N.; Kudin, K. N.; Staroverov, V. N.; Keith, T. A.; Kobayashi, R.; Normand, J.; Raghavachari, K.; Rendell, A. P.; Burant, J. C.; Iyengar, S. S.; Tomasi, J.; Cossi, M.; Millam, J. M.; Klene, M.; Adamo, C.; Cammi, R.; Ochterski, J. W.; Martin, R. L.; Morokuma, K.; Farkas, O.; Foresman, J. B.; Fox, D. J. *Gaussian 16*, Revision A.03, Gaussian, Inc., Wallingford CT, **2016**.

(34) Lazzaroni, R.; Calderone, A.; Lambin, G.; Rabe, J. P.; Brédas, J. L. A Theoretical Approach to the STM Imaging of Adsorbates on the Graphite Surface. *Synth. Met.* **1991**, *41*, 525–528.

(35) Groszek, A. J. Selective Adsorption at Graphite/Hydrocarbon Interfaces. *Proc. R. Soc. London Ser. A* **1970**, *314*, 473–498.

(36) Bléger, D.; Kreher, D.; Mathevet, F.; Attias, A.-J.; Schull, G.; Huard, A.; Douillarad, L.; Fiorini-Debuischert, C.; Charra, F. Surface Noncovalent Bonding for Rational Design of Hierarchical Molecular Self-Assemblies. *Angew. Chem. Int. Ed.* **2007**, *46*, 7404–7407.

(37) Lackinger, M.; Griessl, S.; Heckl, W. M.; Hietschold, M.; Flynn, G. W. Self-Assembly of Trimesic Acid at the Liquid-Solid Interface–a Study of Solvent-Induced Polymorphism. *Langmuir* **2005**, *21*, 4984–4988.

(38) Lei, S.; Tahara, K.; Feng, X.; Furukawa, S.; De Schryver, F. C.; Müllen, K.; Tobe, Y.; De Feyter, S. Molecular Clusters in Two-Dimensional Surface-Confined Nanoporous Molecular Networks: Structure, Rigidity, and Dynamics. *J. Am. Chem. Soc.* **2008**, *130*, 7119–7129.

(39) Fang, Y.; Ghijsens, E.; Ivasenko, O.; Cao, H.; Noguchi, A.; Mali, K. S.; Tahara, K.; Tobe, Y.; De Feyter, S. Dynamic Control over Supramolecular Handedness by Selecting Chiral Induction Pathways at the Solution-Solid Interface. *Nature Chem.* **2016**, *8*, 711–717.

(40) Elke, G.; Ivasenko, O.; Tahara, K.; Yamaga, H.; Itano, S.; Balandina, T.; Tobe, Y.; De Feyter, S. A Tale of Tails: Alkyl Chain Directed Formation of 2D Porous Networks Reveals Odd-Even Effects and Unexpected Bicomponent Phase Behavior. *ACS Nano* **2013**, *7*, 8031–8042.

(41) Yin, S.; Wang, C.; Qiu, X.; Xu, B.; Bai, C. Theoretical Study of the Effects of Intermolecular Interactions in Self-Assembled Long-Chain Alkanes Adsorbed on Graphite Surface. *Sur. Interface Anal.* **2001**, *32*, 248–252.

(42) Keller, T. J.; Bahr, J.; Gratzfeld, K.; Schönfelder, N.; Majewski, M. A.; Stępień, M.; Höger, S.; Jester, S.-S. Nanopatterns of Arylene-Alkynylene Squares on Graphite: Self-Sorting and Intercalation. *Beilstein J. Org. Chem.* **2019**, *15*, 1848–1855.

(43) Gutzler, R.; Sirtl, T.; Dienstmaier, J. F.; Mahata, K.; Heckl, W. M.; Schmittel, M.; Lackinger, M. Reversible Phase Transitions in Self-Assembled Monolayers at the Liquid-Solid Interface: Temperature-Controlled Opening and Closing of Nanopores. *J. Am. Chem. Soc.* **2010**, *132*, 5084–5090.

(44) Song, W.; Martsinovich, N.; Heckl, W. M.; Lackinger, M. Born-Haber Cycle for Monolayer Self-Assembly at the Liquid-Solid Interface: Assessing the Enthalpic Driving Force *J. Am. Chem. Soc*, **2013**, *135*, 14854–14862.

(45) Barnard, R. A.; Matzger, A. J. Functional Group Effects on the Enthalpy of Adsorption for Self-Assembly at the Solution/Graphite Interface. *Langmuir*, **2014**, *30*, 7388–7394.

(46) Mammen, M.; Shakhnovich, E. I.; Whitesides, G. M. Using a Convenient, Quantitative Model for Torsional Entropy to Establish Qualitative Trends for Molecular Processes That Restrict Conformational Freedom. *J. Org. Chem.* **1998**, *63*, 3168–3175.

(47) Mammen, M.; Shakhnovich, E. I.; Deutch, J. M.; Whitesides, G. M. Estimating the Entropic Cost of Self-Assembly of Multiparticle Hydrogen-Bonded Aggregates Based on the Cyanuric Acid·Melamine Lattice. *J. Org. Chem.* **1998**, *63*, 3821–3830.

(49) Yokoyama, S.; Hirose, T.; Matsuda, K. Photoinduced Four-State Three-Step Ordering Transformation of Photochromic Terthiophene at a Liquid/Solid Interface Based on Two Principles: Photochromism and Polymorphism. *Langmuir* **2015**, *31*, 6404–6414.

TOC IMAGE

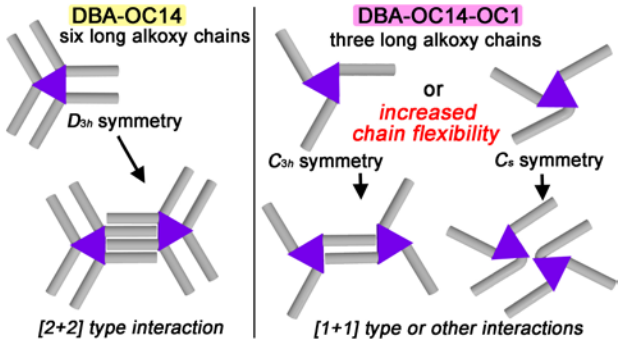
DBA-OC14
six long alkoxy chains
D3h symmetry
[2+2] type interaction
DBA-OC14-OC1
three long alkoxy chains
or
increased
chain flexibility
C3h symmetry
Cs symmetry
[1+1] type or other interactions